NUMERICAL SIMULATION OF SUPERSONIC INTAKE USING STRUCTURED-UNSTRUCTURED ZONAL APPROACH

Masahiro Kanazaki*, Hitoshi Fujiwara*, Yasushi Ito,**
Takeshi Fujita†, Shigeru Obayashi‡, Kazuhiro Nakahashi†
***Institute of Space Technology and Aeronautics, Japan Aerospace Exploration Agency, Japan.**
****** Dept. of Mechanical Engineering, University of Alabama, USA.**
†Department of Aeronautics and Space Engineering, Tohoku University, Japan.
‡Institute of Fluid Science, Tohoku University, Japan.

Keywords: *Engine/Airframe Integration, Supersonic Intake, CFD, Zonal Approach*

Abstract

Numerical simulation method for the prediction of supersonic intake performance is discussed. To perform a practical simulation, it is necessary to consider not only the nacelle-only configuration but also the engine/airframe configuration. In this study, the unstructured mesh, known to have advantages with regard to adaptation to complex geometry, was generated around aircraft geometry and Euler equation was solved. To obtain higher numerical accuracy for the shock wave/boundary layer interaction, which appears at the inlet, the structured Navier-Stokes solver was applied to solve flows inside the flow-through nacelle. These regions were coupled with using the unstructured-structured zonal approach. The nacelle-only configuration and the engine/airframe configuration were calculated using this method and the effects of the airframe existence on supersonic intake performance were investigated.

1 Introduction

A next generation supersonic experimental aircraft with propulsion systems (National EXperimental Supersonic Transport: NEXST2) is currently under development at the Japan Aerospace Exploration Agency (JAXA: the former National Aerospace Laboratory of Japan (NAL)) [1]. In such studies, the engine/airframe integration problem [2] should be considered. Due to the strong interactions among wing, fuselage, and engine nacelle [3, 4], in the design of a highly efficient supersonic intake that can achieve higher pressure recovery and less pressure distortion, its performance should be predicted not only with the nacelle-only configuration but also with the engine/airframe configuration with changing mass flow ratio inside the nacelle to simulate an actual engine.

In this study, intake performances are evaluated by pressure recovery and distortion index. The pressure recovery indicates the efficiency of the engine operation and the uniformity of the pressure distribution at the end of the intake. They are defined as:

$$\text{(Pressure recovery)}\ (\%) = 100 \times p_{0out}/p_0 \qquad (1)$$

$$\text{(Distortion index)}\ (\%) = 100 \times (p_{0max,out} - p_{0min,out})/p_0 \qquad (2)$$

where, p_0 is the total pressure of the mainstream, p_{0out} is the average value of the total pressure at the end of the diffuser. $p_{0max,out}$ and $p_{0min,out}$ are the maximum pressure and the minimum pressure at the end of the diffuser, respectively.

Wind tunnel tests performed by NAL (Fig. 1) measured the pressure recovery to invest the stability range. This test indicated that the stability range of the engine/airframe configuration was decreased by about 5% as compared with the nacelle-only configuration as shown in Fig. 2. It revealed that the supersonic intake performance was affected by the airframe existence. To study the cause of the difference, the simulation of the nacelle-only configuration and engine/airframe configuration were preformed and calculative results were compared.

To predict intake performance correctly, the shock interaction to the boundary layer and the separation at the intake ramp should be calculated by a high order scheme. In previous

study [5], Navier-Stokes simulation with the low Reynolds number *k-ε* turbulent model using the structured grid method was applied to the nacelle-only configuration and it showed a high degree of numerical accuracy. On the other hand, it is difficult to apply the structured grid method to complex geometry, such as the engine/airframe configuration. Therefore, the unstructured grid method is often used to adapt such complex geometry [3, 6]. However, the unstructured grid method has difficulties in obtaining a high degree of accuracy near the boundary layer. The hybrid prismatic/tetrahedral unstructured grid method for viscous flow was proposed [7], but the structured grid method still has advantages when applied to simple geometry, such as inside the flow through a nacelle with a high-order scheme using the turbulent model [8].

In this study, a structured grid-unstructured grid zonal approach was developed to predict the supersonic intake performance of the engine/airframe configuration. In this approach, the computational domain was decomposed into two sub-domains; inside the flow-through nacelle from supersonic intake and outside the aircraft integrated engine nacelle. For inside the flow-through nacelle, a structured grid method [9] was used for highly accurate simulation of the boundary layer at the intake. For the outer flow around the aircraft, the unstructured grid method [10] was applied to adapt the complex aircraft geometry. The Navier-Stokes code with the low Reynolds number *k-ε* turbulent model [11] was solved for the structured domain and the Euler code [12] was solved for the unstructured domain assuming that the boundary layer effect is not strong for external flows around the aircraft. To exchange state variables between structured grid and unstructured grid domains, the structured-unstructured zonal approach [13] was developed with the introduction of a one-mesh overlap interface. To simulate actual flights, nacelle mass flow ratios must be controlled. The throat was introduced to the flow-through nacelle of the structured domain, and the nacelle mass flow ratios can be controlled by changing the height of the throat.

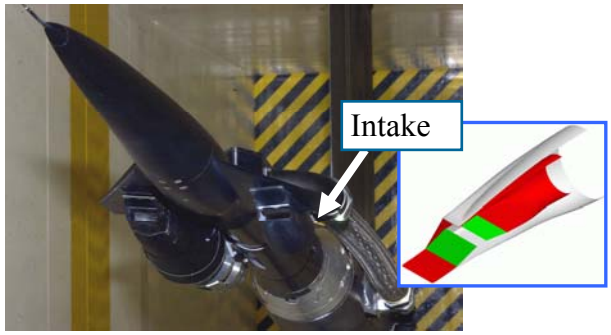

Fig. 1 Wind tunnel model 02 for scaled supersonic experimental aircraft and intake model.

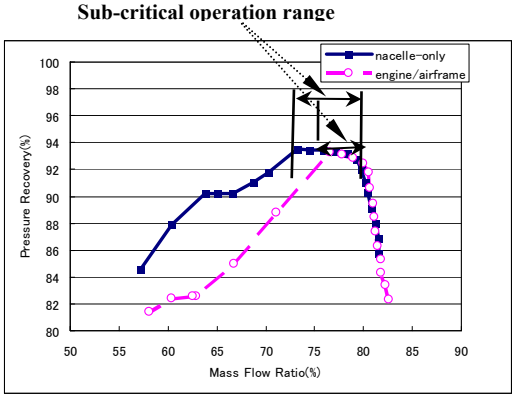

Fig. 2 Experimental results of pressure recovery *vs*. nacelle mass flow ratio obtained by nacelle-only configuration and engine/airframe configuration.

2 Structured-Unstructured Zonal Approach

2.1 Structured Grid Navier-Stokes Solver with Low Reynolds Number *k-ε* turbulent model

For accurate simulation of the shock wave and the boundary layer interaction near the intake, the structured multi-block grid and the high order viscous flow solver were applied [5, 10]. The computational domain was decomposed into three sub-domains as shown in Fig. 3 and 170×99×27 points for domain 1, 170×25×25 points for domain 2, and 105×65×46 points for domain 3, which is a cavity, and the Navier-Stokes equation with the low Reynolds number *k-ε* turbulent model [11] was solved. The governing equation in the differential form is written as:

$$\frac{\partial \mathbf{Q}}{\partial t} = -\frac{1}{x_l}\left(\mathbf{F}(\mathbf{Q})_l - \frac{1}{\mathrm{Re}}\mathbf{G}(\mathbf{Q})_l\right) \tag{3}$$

where $\mathbf{Q}=[\rho,\rho u,\rho v,\rho w,e]^{\mathrm{T}}$ is the vector of conservative variables; ρ is the density; u, v, and w are the Cartesian velocity components; and e is the total energy. The vectors $\mathbf{F}(\mathbf{Q})$ and $\mathbf{G}(\mathbf{Q})$ represent the inviscid flux vector and viscous flux vector.

Spatial differences were evaluated by a third-order upwind biased Roe scheme [12, 13] with a TVD limiter of Chakravathy and Osher type [14]. For time advancement, a second-order Runge-Kutta scheme was used.

To control nacelle mass flow ratios, the throat was introduced to the flow-through nacelle of the structured domain as shown in Fig. 3. The nacelle mass flow ratios are controlled by changing the area ratio of the throat as described in the previous chapter [3, 5].

Low Reynolds number k-ε turbulent model

Low Reynolds number k-ε turbulent model [11] can be written as:

$$\begin{aligned}
&\frac{\partial}{\partial t}(\rho k)+\frac{\partial}{\partial x_l}\left\{\rho k u_l-\left(\mu+\frac{\mu_t}{\sigma_k}\right)\frac{\partial k}{\partial x_l}\right\}=P-\rho\varepsilon \\
&\frac{\partial}{\partial t}(\rho \varepsilon)+\frac{\partial}{\partial x_l}\left\{\rho \varepsilon u_l-\left(\mu+\frac{\mu_t}{\sigma_\varepsilon}\right)\frac{\partial \varepsilon}{\partial x_l}\right\}=C_1 P\frac{\varepsilon}{k}-C_2 f_2 \rho\frac{\varepsilon^2}{k}
\end{aligned} \tag{4}$$

where

$$\begin{aligned}
&P=\mu_t S-\frac{2}{3}\rho k D \\
&S=\left(\frac{\partial u_m}{\partial x_l}+\frac{\partial u_l}{\partial x_m}\right)\frac{\partial u_m}{\partial x_l}-\frac{2}{3}D^2 \\
&D=\frac{\partial u_m}{\partial x_m} \\
&\mu_t=C_\mu f_\mu \frac{\rho k^2}{\varepsilon}
\end{aligned} \tag{5}$$

f_μ, f_2 are supplementary coefficients for wall boundary and low Reynolds effect, respectively. C_1, C_2, σ_k, σ_ε are model coefficients, which many kind of models are proposed. In this study, Myong-Kasagi model is used. Myong-Kasagi model is written as:

$$\begin{aligned}
&f_\mu=\left\{1-\exp\left(-\frac{y^+}{70}\right)\right\}\left(1+\frac{3.45}{\sqrt{R_t}}\right) \\
&f_2=\left[1-\frac{2}{9}\exp\left\{-\left(\frac{R_t}{6}\right)^2\right\}\right]\left\{1-\exp\left(-\frac{y^+}{5}\right)\right\}^2 \\
&R_t=\frac{\rho k^2}{\mu\varepsilon} \\
&\rho_k=1.4,\quad \rho_\varepsilon=1.3, \\
&C_\mu=0.09,\quad C_1=1.4,\quad C_2=1.8
\end{aligned} \tag{6}$$

In this study, boundary conditions of k and ε are used as follows:

$$\begin{aligned}
&k=0 \\
&\varepsilon=2\nu\left(\frac{\partial\sqrt{k}}{\partial y}\right)^2
\end{aligned} \tag{7}$$

2.2 Unstructured Euler Solver

For simulation of flow around the aircraft, the unstructured grid method was applied to adapt the complex geometry as shown in Fig. 4. In this study, it was assumed that the effect of the boundary layer around the outside of the aircraft on the supersonic intake spaced from the lower wing by a diverter was not particularly strong [15]. Therefore, the flowfield around the aircraft was calculated by the Euler equations written as:

$$\frac{\partial}{\partial t}\int_\Omega \mathbf{Q}dV+\int_{\partial\Omega}\mathbf{F}(\mathbf{Q})\cdot\mathbf{n}dS=0 \tag{8}$$

where $\mathbf{Q}=[\rho,\rho u,\rho v,\rho w,e]^{\mathrm{T}}$ is the vector of conservative variables; ρ is the density; u, v, and w are the Cartesian velocity components; and e is the total energy. The vectors $\mathbf{F}(\mathbf{Q})$ represent the inviscid flux and $\mathbf{n}$ is the outward normal of $\partial\Omega$, which is the boundary of the control volume Ω. Equations (8) were solved by a finite-volume cell-vertex scheme.

The Harten-Lax-van_Leer-Einfeldt-Wada (HLLEW) Riemann solver [16] was used for the numerical flux computations. A numerical limiter was used to prevent overshoots of the interpolated solution during the flux computation. Here, Venkatakrishnan's limiter [17] was used because of its superior convergence properties. For time integration,

the lower-upper symmetric Gauss-Seidel (LU-SGS) implicit method [18], originally developed for a structured grid method and rewritten for the unstructured grid method, was applied.

2.3 Grid Generation at Interface

In this study, the computational domain was decomposed into two sub-domains; the structured grid region inside the nacelle and the unstructured grid region around the engine/aircraft configuration. Therefore, state variables need to be exchanged between them, and an structured-unstructured zonal approach using a one-mesh overlap was developed [9].

In Ref. 9, a structured grid was used around some objects independently to simulate the boundary layer accurately and the unstructured grid finite element method (FEM) was used to joint all structured regions using the zonal approach. However, in this study, the structured grid finite differential method (FDM) was applied to the flow-through nacelle to obtain numerical accuracy of the shock wave appearing near the inlet, and the unstructured finite volume method (FVM) was applied to the outer flow of the aircraft. Then, to joint the two regions, the zonal approach was also considered in this study.

In this study, a tetrahedral unstructured grid for outer flow of the aircraft was generated. The present grid generation process was streamlined to start from CAD data using CATIA [19], then to generate a surface grid applying the advancing-front method [20], and finally to generate a volume grid [21]. The volume grid was generated in two steps. First, Delaunay Triangulation [22] was applied from the surface grid to generated isotropic tetrahedral elements. Second, vertexes were added to generate the overlapping tetrahedral elements on the interface as illustrated in Fig. 5. As the structured elements in front of the intake near the interface should be thin rectangles from the intake boundary layer for FDM, to avoid the extreme thin tetrahedral elements, vertexes for the interface of the unstructured grid were put on thinned-out points in the j direction of the structured region as shown in Fig. 5. The j direction was not the main stream, so there was less influence on accuracy in exchanging state variables between two regions.

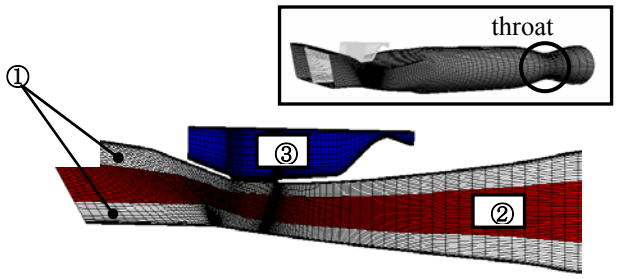

Fig. 3 Generated structured grid for intake and flow-through nacelle with throat.

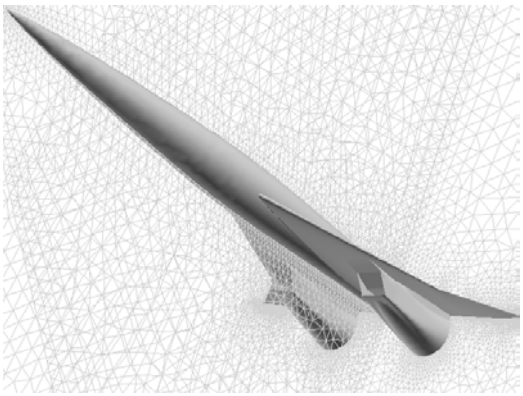

Fig. 4 Generated unstructured grid around scaled supersonic airplane model.

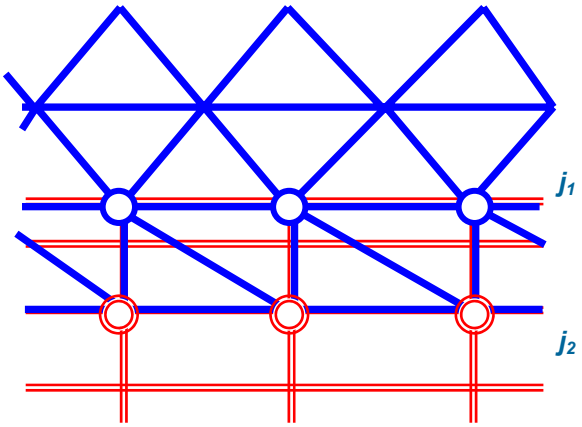

Fig. 5 One mesh overlapped grid for structured-unstructured zonal approach.

3 Results

In this study, predictions of supersonic intake performance for the nacelle-only configuration

and the engine/airframe configuration were made using the structured-unstructured zonal approach and computational results were compared to investigate the effects of the airframe. Solutions were obtained at a freestream Mach number, M_∞=2, and angle of attack, 0 deg. For the structured grid region inside the nacelle, Reynolds number was determined to be 0.866×10^6 normalized by the height of the capturing area of the intake. In this study, the heights of the throat shape were set to 36%, 36.5%, 37%, 38%, 40%, 42%, 44%, and 46% of the nacelle outlet radius.

The calculation time was about 60-120 hours (convergence time was dependent on the mass flow ratio) using a single CPU on the Numerical Simulator 3 (NS3) [23] at JAXA per case.

3.1 Verification of Computational Grid by Structured-Unstructured Zonal Approach

Figure 6 shows the present computational grid for the structured-unstructured zonal approach and the Mach number contour line is illustrated in Fig. 7. This figure shows that the exchange of state variables between the structured and unstructured domain was carried out appropriately. The contour at the main stream of the engine/airframe configuration was different from the nacelle-only configuration because of the presence of the wing and the fuselage. This difference should influence the intake performance of the engine/airframe configuration and cause differences in the intake performance between the engine/airframe configuration and the nacelle-only configuration.

Figure 8 shows a comparison of the total pressure variation normalized by the main stream total pressure obtained by the present method and the previous structured grid method [5] using the structured grid for the outer region along the direction from the intake ramp to the end of the intake. These results were identical and suggested that the present method using the unstructured grid to calculate the outer region was appropriate in comparison with the structured solver reported previously.

Figures 9 (a) and (b) show comparisons of the nacelle-only configuration and the engine/airframe configuration with wind tunnel tests, respectively. The computational results shown in Fig. 9 (a) indicate a slight difference in the critical point for instability of the intake flow called “buzz” [24-26]. However, the sub-critical operation range, which maintains high pressure recovery in that the intake can provide sufficient air to the turbo-fan engine during operation, showed good agreement with the experimental results. On the other hand, the sub-critical operation range was decreased as compared with the nacelle-only configuration, as shown in Fig. 9 (b), and the same tendency was found in the experimental results. However, the numerical results did not agree well with those of the experiment especially about the critical point for the buzz.

This disagreement might have been caused by the accuracy of the wind tunnel test. The scale of the intake models for the nacelle-only configuration ($Re=1.38\times10^6$) and the engine/airframe configuration ($Re=0.89\times10^6$) were different, and this might have caused the experimental error in the model shape when the intake model was made for the engine/airframe configuration. Measurement of mass flow inside the flow-through nacelle was very sensitive and it may lead to the experimental error in determining the mass flow ratio. On the other hand, the computational results with the fine unstructured mesh of the engine/airframe configuration (1,450,638 tetrahedral elements) calculated at 77% mass flow ratio were identical to those obtained with the original mesh, as shown in Fig. 9 (b). This suggests that the grid resolution had sufficient quality to obtain numerical accuracy.

3.2 Mach Number Variation with Changing Mass Flow Ratio of Engine/Airframe Configuration

Figure 10 shows a comparison of the computed Mach number contours about the engine/airframe configuration at four mass flow ratios (79%, 77%, 73%, and 70%). These figures indicate that the normal shock wave that

appeared at the end of the intake moved upstream as the mass flow ratio decreased.

When the mass flow ratio was kept fairly large, the normal shock stops behind the intake ramp as shown in Fig. 10 (a) and the turbo-fun engine can work well with a stable flow inside the nacelle. On the other hand, when the mass flow ratio becomes small and the normal shock emerges from the edge of the nacelle's cowl, the normal shock wave interacts with the oblique shock wave from the intake ramp. This produces the triple-point in front of the intake and also produces the slip line into the nacelle duct (Figs. 10 (b) and (c)). In this simulation, although the triple-point appeared near the interface between the structured region and the unstructured region, the present method successfully captured such a complex interaction.

Figure 10 (d) shows the case of the smallest mass flow ratio in these pictures. In this case, the slip line affects the end of the intake and the shock wave oscillates near the intake. Then, it causes instability in the intake flow, which would adversely affect operation of the turbo-fan's engine.

3.3 Comparison the Computational Performance of Nacelle-Only Configuration and Engine/Airframe Configuration

Figure 11 shows a comparison of the total pressure recovery of the nacelle-only configuration and the engine/airframe configuration at various mass flow ratios. The total pressure recovery decreased at the critical point in each case, as the mass flow ratio decreased. However, the sub-critical operation range of the engine/airframe configuration became almost 4% smaller than the nacelle-only configuration, as shown in Fig. 11. These results suggest that the nacelle-only configuration can lead to a more uniform flow to the turbo-fan engine than the engine/airframe configuration. This tendency agreed with the results of wind tunnel tests performed by JAXA (the former NAL).

Figure 12 illustrates total pressure distributions (normalized by the total pressure of the main stream) of the cross-section in front of the intake and the end of the intake at the mass flow ratio of the critical point. As the slip line produced by the triple-point of the shock wave and the separation of the boundary layer by the intake ramp, distributions at the nacelle duct (A-A') were not uniform in each case. In the case of the nacelle-only configuration, the distribution became symmetrical. On the other hand, in the case of the engine/airframe configuration, the distribution became asymmetrical. This was caused by the main stream to the intake changed by the interaction of the fuselage and the wing. This asymmetrical distribution was the cause of the narrow sub-critical operation range in the engine/airframe configuration.

The integrated engine/airframe configuration has 1 degree toe-in angle for the nacelle installation. The toe-in angle was introduced to avoid the leading-edge contamination from the relatively large nacelle compared to the airframe. To investigate the detail, the nacelle-only configuration with 1 degree slip-angle was also calculated. In this case, the sub-critical operation range was decreased similar to the case of the engine/airframe configuration as shown in Fig. 11. In this case, the uniform pressure distribution was given at the intake because the airframe does not exist. Therefore, the pressure distribution at the end of the intake was not same as the engine/airframe configuration. However, because of the slip-angle, the pressure distribution became asymmetrical at the end of the intake and larger separation was produced, which promotes the shear generation. This result suggests that the toe-in angle of the intake is caused of the promotion of the shear generation and the decreasing of the sub-critical operation range.

According these results, the intake performance seems to be affected only by the toe-in angle not by airframe existence. However, as shown in Table 1, the distortion index of the engine/airframe integration is the largest among the three cases. This result shows that the airframe existence increases the distortion index

and thus the pressure distribution at the end of the engine intake is most disturbed.

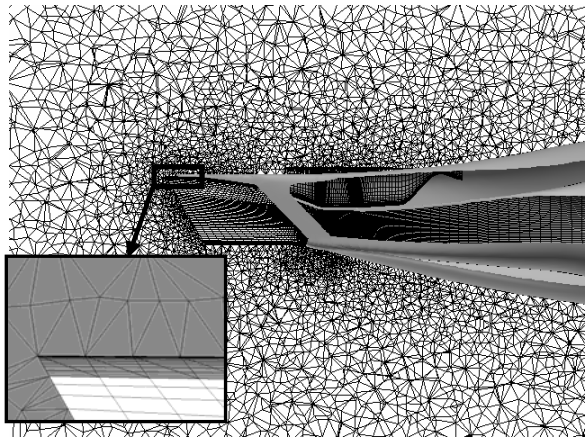

Fig. 6 Final computational grid for structured-unstructured zonal approach.

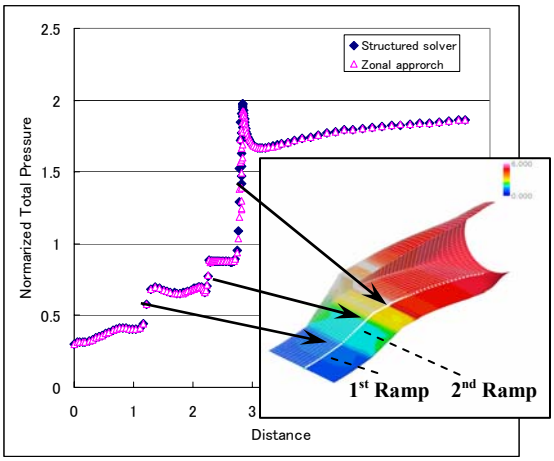

Fig. 7 Comparison of total pressure distribution along intake centerline obtained by nacelle-only configuration using the original structured solver and the developed structured-unstructured zonal approach.

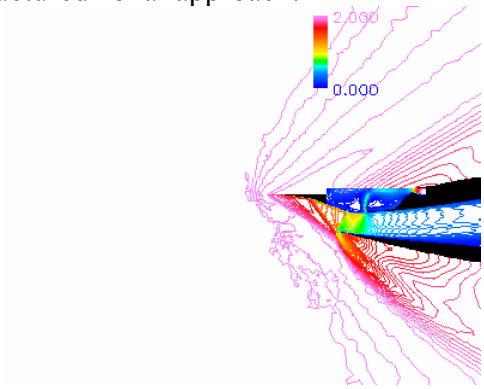

(a)

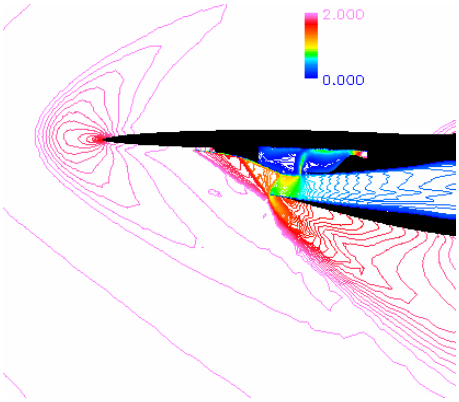

(b)

Fig. 8 Computed Mach number contours along a cross sectional view of the nacelle; (a) nacelle-only configuration, (b) wing-body-nacelle configuration.

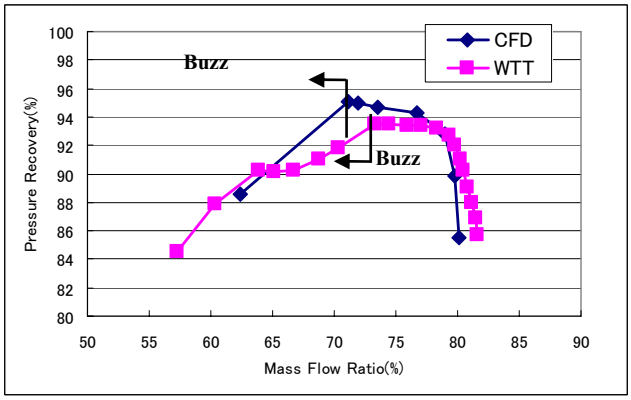

(a)

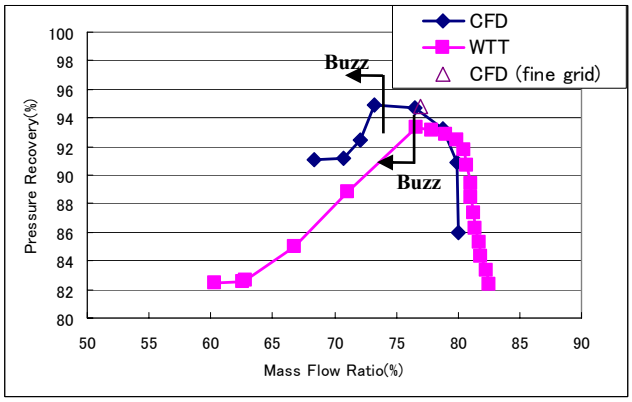

(b)

Fig. 9 Comparison of computational results with experiment: (a) nacelle-only configuration, (b) engine/airframe configuration.

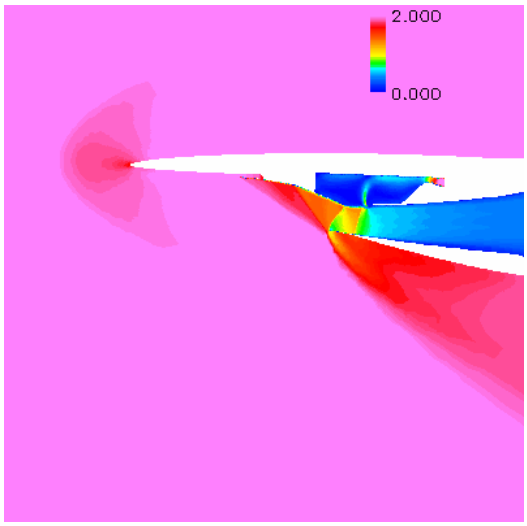

(a)

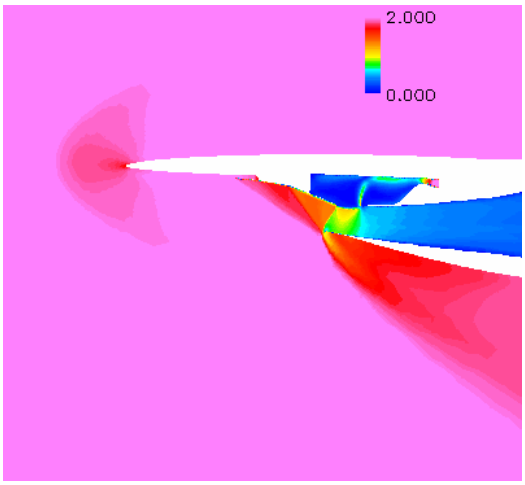

(b)

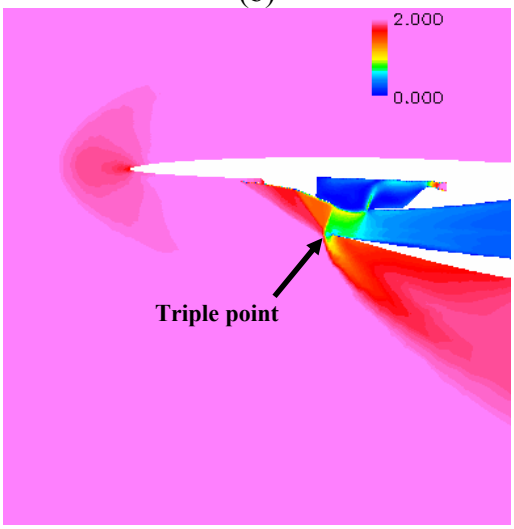

(c)

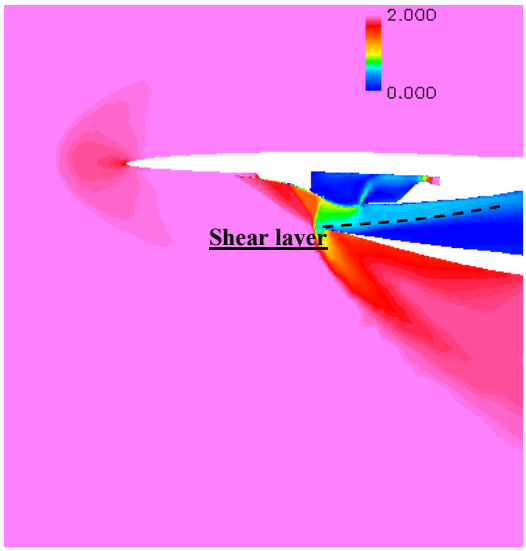

(d)

Fig. 10 Computed Mach number contours of wing-body-nacelle configuration along a cross sectional view of the nacelle; (a) MFR79%, (b) MFR77%, (c) MFR73%, (d) MFR66%.

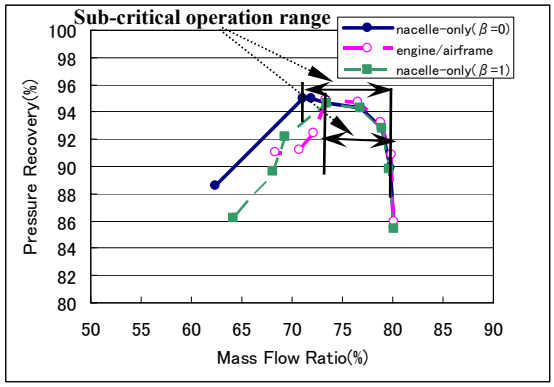

Fig. 11 Comparison of computational results obtained by nacelle-only configuration and engine/airframe configuration.

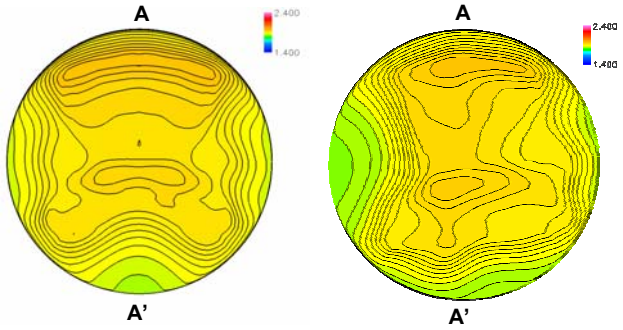

(a) (b)

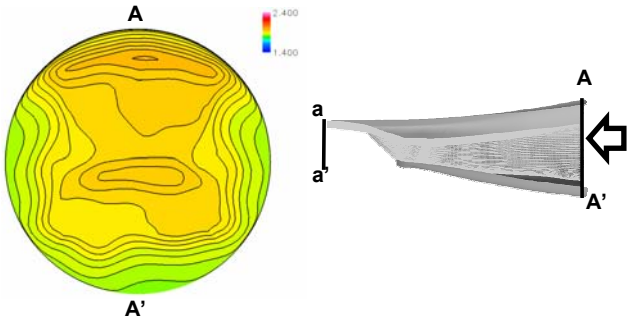

(c)

Fig. 12 Cross-sectional view of total pressure distribution at end of the intake: (a) nacelle-only configuration (β=0 deg.), (b) engine/airframe configuration and (c) nacelle-only configuration (β=1 deg.)

Table 1 Computational pressure recovery and distortion index.

configuration	nacelle-only (α=1°)	nacelle-only (α=1°)	engine/airframe
Pressure Recovery (%)	95.02%	94.67%	94.94%
Distortion index (%)	7.23%	**7.10%**	**7.85%**

4 Conclusions

The prediction of supersonic intake performance using the numerical simulation code with the structured-unstructured zonal approach was performed. In this study, the flowfield was divided into two domains; inside the nacelle and outside of the aircraft. The flowfield inside the nacelle was simulated by solving the Navier-Stokes equation with the structured grid method to obtain a high degree of accuracy concerning the boundary layer at the intake. On the other hand, the flowfield around the engine/airframe configuration was simulated by solving the Euler equations with the unstructured grid method to adapt the complex geometry under the assumption that the effect of the boundary layer around the aircraft is not important. To exchange the state variables between these regions, the structured-unstructured zonal approach was developed.

The present method was able to predict not only the intake performance of the nacelle-only configuration but also that of the engine/airframe configuration while maintaining a high degree of accuracy. The shock wave movement near the intake was also observed. Remarkably, the interaction of the normal shock from the flow-through nacelle and the oblique shock generated at the intake ramp, so-called the triple point, was captured clearly.

In this study, the intake performance was evaluated by the pressure recovery at various mass flow ratios. The sub-critical operation range of the engine/airframe configuration became smaller than that of the nacelle-only configuration. This suggested that the presence of wing and fuselage affected the flowfield inside the nacelle. This tendency agreed with the experimental observations. However, the critical points for "buzz" did not agree well with the experimental results, especially in case of the engine/airframe configuration. In future studies, the quality of the wind tunnel test should be considered and parametric analysis with changes in mass flow ratio and the slip angle should be performed to investigate the phenomena in more detail.

5 References

[1] Sakata, K., "Supersonic Experimental Airplane (NEXST) for Next Generation SST Technology," AIAA Paper 2002-0527, 2002.

[2] Li, J., Li, F., and Qin, E., "Numerical Simulation of Transonic Flow over Wing-Mounted Twin-Engine Transport Aircraft," *J. of Aircraft*, Vol. 37, No. 3, pp. 469-478, 2000.

[3] Kanazaki, M., Obayashi, S. and Nakahashi, K., "Numerical Simulation of Supersonic Flow around Wing-Body Configuration with Integrated Engine Nacelle," *AIAA J.,* Vol. 41, No.2, pp. 213-217, 2002.

[4] Seddon, J. and Goldsmith, E. L. "Intake Aerodynamics," AIAA Education Series 1985.

[5] Fujiwara, H., Murakami, A. and Watanabe, Y., "Numerical Analysis on Shock Oscillation of Two-Dimensional External Compression Intakes," AIAA Paper 2002-2740, 2002.

[6] Kanazaki, M., Morikawa, M., Obayashi, S. and Nakahashi, K., "Exhaust Manifold Design for a Car Engine Based on Engine Cycle Simulation," *Proc. of International conference Parallel CFD2002*, 2002.

[7] Sharov, D. and Nakahashi, K., "Reordering of 3-D Hybrid Unstructured Grids for Lower-Upper Symmetric Gauss-Seidel Computations," *AIAA J.*, Vol. 36, pp.484-486, 1998.

[8] Wurtzler, K. E., Tomaro, R. F. and Witzeman, F. C., "Analysis of Three Unstructured Grid Techniques from a User's Perspective," *Proc. of the 7th International Conference on Numerical Grid Generation in Computational Field Simulations*, pp.357-366, 2000.

[9] Nakahashi, K. and Obayashi, S., "FDM-FEM Zonal Approach for Viscous Flow Computations over Multiple-Bodies," AIAA Paper 87-0604, 1987.

[10] National Astronomical Obsevatory of Japan edition, *Chronological Scientific*, 1995.

[11] Myong, H. K. and Kasagi, N., "A new approach to the improvement of k-epsilon turbulence model for wall-bounded shear flow," *JSME International J. of Fluid Engineering*, Vol. 109, pp.156-160, 1990.

[12] Roe, P. L., "Approximate Riemann solver, parameter vectors and difference schemes," *J. of Computational Physics*, Vol. 43, pp.357-372, 1981.

[13] Chakravarythy, S. R., "High resolution upwind formulations for the Navier-Stokes equations," *VKI Lecture Series 1988-05*, Computational fluid dynamics, 1988.

[14] Chakravarthy, S.R. and Osher, S., "A new class of high accuracy TVD schemes for hyperbolic conservation laws," AIAA paper 85-0243, 1985.

[15] Fujita, T., Ito, Y., Nakahashi, K. and Iwamiya, T., "Computational Fluid Dynamics Evaluation of National Aerospace Laboratory Experimental Supersonic Airplane in Ascent," *J. of Aircraft*, Vol. 39, No. 2, pp.359-364, 2002.

[16] Obayashi, S. and Guruswamy, G. P., "Convergence Acceleration of an Aeroelastic Navier-Stokes Solver," *AIAA J.*, Vol. 33, No. 6, pp. 1134-1141, 1995.

[17] Venkatakrishnan, V., "On the Accuracy of Limiters and Convergence to Steady State Solutions," AIAA Paper 93-0880, 1993.

[18] Jameson, A. and Turkel, E., "Implicit Schemes and LU Decompositions," *Mathematics of Computation,* Vol. 37, No. 156, pp.385-397, 1981.

[19] Fujita, T., Ito, Y., Nakahashi, K., and Iwamiya, T., "Aerodynamics Evaluation of NAL Experimental Supersonic Airplane in Ascent using CFD," AIAA Paper 2000-0806, 2001.

[20] Ito, Y. and Nakahashi, K., "Direct Surface Triangulation Using Stereolithography Data," *AIAA J.*, Vol. 40, p.p. 490-496, 2002.

[21] Sharov. D. and Nakahashi, K., "Hybrid Prismatic / Tetrahedral Grid Generation for Viscous Flow Applications," *AIAA J.*, Vol. 36, No2, pp.157-162, 1998.

[22] Sharov, D. and Nakahashi, K., "A Boundary Recovery Algorithm for Frlaunay Tetrahedral Meshing," *Proc. of the 5th International Conference on Numerical Grid Generation in Computational Field Simulations*, pp. 229-238, 1996.

[23] Matuo, Y., *et. al.*, "Numerical Simulator III-Building a Terascale Distributed Parallel Computing Environment for Aerospace Science and Engendering," *Proc. of PPSN 2002*, *NORTH-HOLLAND*, pp. 187-194, 2003.

[24] Ferri, A and Nuxxi, L. M. "The origin of aerodynamic instability of supersonic inlets at subcritical condition," NACA, RM L50 K30, 1951.

[25] Fisher, S. A., Neale, M. C. and Brooks, A. J. "On the subcritical stability of variable ramp intakes at Mach numbers around 2," NGTE Report R3111, 1970.

[26] Dailey, C. L., "Supersonic Diffser Instability," *J. of the Aeronautical Sciences*, Vol. 22, No. 11, 1955.

[27] Shipman, J., Cavallo, P. and Hosangadi, A., "Efficient Simulation of Aircraft Exhaust Plume Flows Using A Multi-element Unstructured Methodology," AIAA Paper 2001-0598, 2001.